PAPER

Photocatalytic reduction of carbon dioxide to methanol using a ruthenium trinuclear polyazine complex immobilized on graphene oxide under visible light irradiation†

Pawan Kumar, Bir Sain and Suman L. Jain*

A ruthenium trinuclear polyazine complex was synthesized and subsequently immobilized through complexation to a graphene oxide support containing phenanthroline ligands (GO-phen). The developed photocatalyst was used for the photocatalytic reduction of CO_2 to methanol, using a 20 watt white cold LED flood light, in a dimethyl formamide–water mixture containing triethylamine as a reductive quencher. After 48 h illumination, the yield of methanol was found to be 3977.57 ± 5.60 µmol g_{cat}^{-1}. The developed photocatalyst exhibited a higher photocatalytic activity than graphene oxide, which provided a yield of 2201.40 ± 8.76 µmol g_{cat}^{-1}. After the reaction, the catalyst was easily recovered and reused for four subsequent runs without a significant loss of catalytic activity and no leaching of the metal/ligand was detected during the reaction.

Carbon dioxide (CO_2) is an extremely stable molecule, which is generally produced by the combustion of fossil fuels and respiration. The recycling of CO_2 to form useful products by activation/reduction is a challenging task, requiring appropriate catalysts and energy input. In this context, visible light-driven photoreduction of CO_2 to high energy products, such as methanol, may provide a solution for both the shortage of fossil fuels and global warming.[1] Many semiconductors, such as TiO_2, ZnO, and CdS, have been known to act as photocatalysts for CO_2 reduction, albeit with the major drawbacks of lower quantum yields and poor selectivities.[2] Molecular catalysis using transition metal complexes, such as rhenium(I) bipyridine, ruthenium(II) polypyridine carbonyl, cobalt(II) trisbipyridine, and cobalt(III) macrocycles, as catalysts with a photosensitizer can reduce CO_2 with a relatively high quantum yield and high selectivity of products.[3] However, the homogeneous nature of these catalysts makes the process unviable from economical as well as environmental viewpoints. This problem can be solved by the anchoring of these complexes to a photoactive support, which not only enables the facile recovery of the catalyst, but may also allow the photoactive support and complexes to work synergistically for better electron transfer to CO_2.[4]

Since the discovery of graphene in 2007,[5] it has been developed rapidly because of its excellent physical properties,

including its excellent thermal conductivity, high mechanical strength and carrier mobility, and fascinating chemical properties.[6a–c] Owing to the presence of ample oxygen-containing functionalities and its high surface area, it has emerged as a promising material for the heterogeneization of homogeneous metal complexes.[7a–c] Metal-free graphene-based materials, due to their surface charge separation abilities, can serve as catalysts in energy production applications.[8] In this context, Hsu *et al.* reported the use of graphene oxide as a photocatalyst for CO_2 reduction, however the yield was 0.172 µmol g_{cat}^{-1} h^{-1}.[9] The yield can further be increased by the anchoring of visible light-absorbing molecules to the graphene oxide support.[10] In the present paper, we have used ruthenium polyazine complexes as anchoring units as they strongly absorb visible light and, by changing the ligand and the number of complex units, the absorption range can be tuned.[11] We have synthesized ruthenium trinuclear polyazine complexes and then anchored these to the graphene oxide support through complex formation with phenanthroline ligands. The synthesized photocatalyst was used for the photoreduction of CO_2 to methanol under visible light irradiation, and provided a methanol yield of 3977.57 ± 5.60 µmol g_{cat}^{-1} after 48 h in the presence of triethylamine as a sacrificial donor.

Synthesis and characterization of the catalyst

Graphene oxide was prepared by the oxidation of graphite under harsh conditions, by following a modified Hummers method.[12] The high specific surface area and easy access to

Chemical Sciences Division, CSIR-Indian Institute of Petroleum Mohkampur, Dehradun-248005, India. E-mail: suman@iip.res.in; Fax: +91-135-2660202; Tel: +91-135-2525788

oxygen-containing functionalities on the surface of the graphene oxide sheets enables the facile immobilization of the metal complexes on the graphene oxide support. Prior to immobilization, the GO was treated with chloroacetic acid to convert the OH and epoxy groups to –COOH groups, which were subsequently treated with thionyl chloride and then used for the grafting of the 1,10-phenanthroline-5-amine ligands to the GO surface. Ruthenium trinuclear complex **1** was synthesized by following a literature procedure, as shown in Scheme 1. Finally, the trinuclear complex **1** was immobilized *via* complexation with the phenanthroline ligands grafted on the surface of graphene oxide. The schematic representation of the synthesis of the ruthenium(II) trinuclear complex immobilized on graphene oxide (Ru–phen-GO) **2** is shown in Scheme 2.

The N_2 adsorption–desorption isotherms of **2** are depicted in Fig. S1.† The supported material retains the characteristics of a type IV isotherm and mesoporosity.[13] The BET surface area (S_{BET}), total pore volume (V_P) and mean pore diameter (r_p) for GO were found to be 85.54 m^2 g^{-1}, 0.1123 cm^3 g^{-1} and 5.5566 nm, respectively (Fig. S2a†). The S_{BET} of **2** was 27.961 m^2 g^{-1}, which was assumed to be due to the successful attachment of the complex to the surface of GO. The total pore volume and mean pore diameter of **2** were 0.1089 cm^3 g^{-1} and 15.577 nm, respectively (Fig. S2b†). The changes in the surface properties of GO confirmed the successful attachment of the ruthenium complexes to the GO surface.

XRD patterns were used to study changes in structure (Fig. 1). The XRD spectrum of GO, as shown in Fig. 1a, gives a characteristic diffraction peak at 10.80 (001), related to the GO interlayer spacing of approximately 0.74 nm.[14] After immobilization of the ruthenium complex **1**, this peak disappeared and another broad diffraction peak for graphite (002) at 2θ value ∼26° appeared, indicating that exfoliation of the layered Ru–phen-GO was achieved.[15] The XRD pattern clearly indicates that the material was amorphous in nature.

The surface morphologies of GO and Ru–phen-GO were investigated *via* scanning electron microscopy (SEM) and transmission electron microscopy (TEM). The SEM image of GO (Fig. 2a) exhibited typical two-dimensional, multilayered nanosheets with macroscopic wrinkling, as documented in the literature. The SEM image of Ru–phen-GO **2** (Fig. 2b) exhibited an agglomerated, layered structure incorporating macromolecular complex moieties between the sheets. The EDX pattern
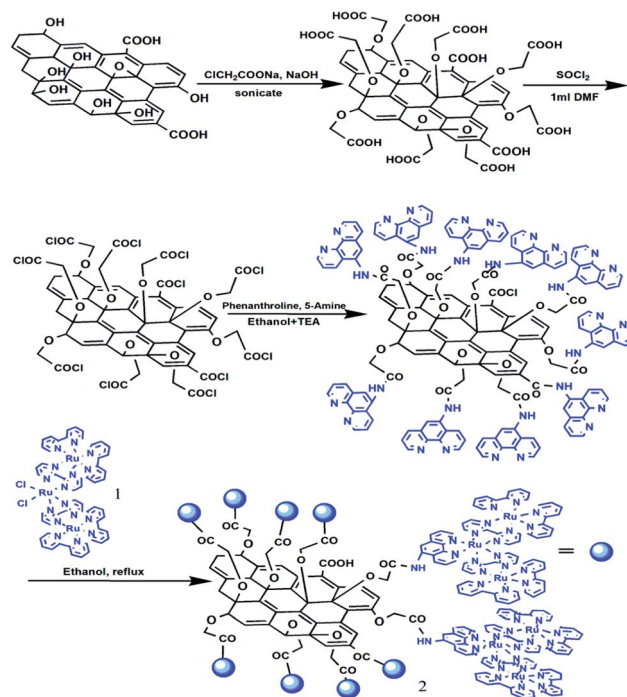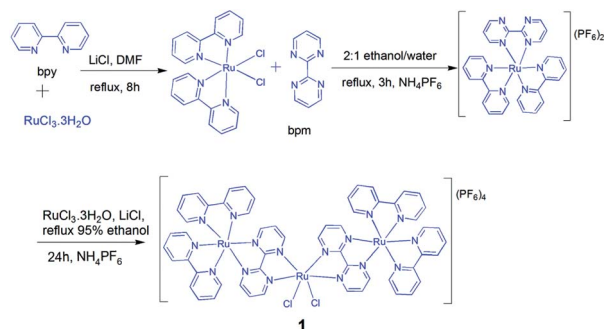

Scheme 2   Synthesis of Ru–phen-GO **2**.

clearly indicates the presence of the ruthenium complex in the synthesized material **2** (Fig. 2c).

The TEM images of **2** show twisted and crumpled nanosheets (Fig. 3). It can be seen that the crumpled nanosheets are in an agglomerated phase. Furthermore, the appearance of dark spots indicates that the ruthenium complexes were successfully grafted to the GO nanosheets (Fig. 3b). In addition, the ruthenium complex moieties were intercalated between GO's sheets and the morphology of the sheets remained intact during the immobilization of the complex. The selected area electron diffraction (SAED) pattern of the catalyst shows that the material was amorphous in nature (Fig. 3c).

Fig. 4 shows the FT-IR spectra of the ruthenium trinuclear complex **1**, GO and GO-supported complex **2**. The pure support GO (Fig. 4b) exhibited bands at 3409, 1720, 1621, 1220, and 1058 cm^{-1} due to the stretching modes of the O–H, C=O, C=C, C–O

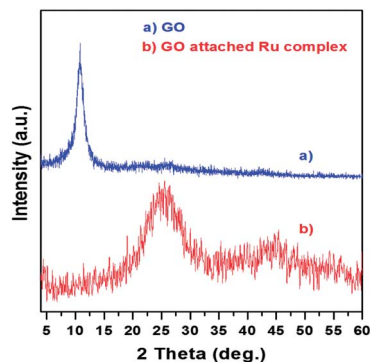Scheme 1   Synthesis of ruthenium trinuclear complex **1**.

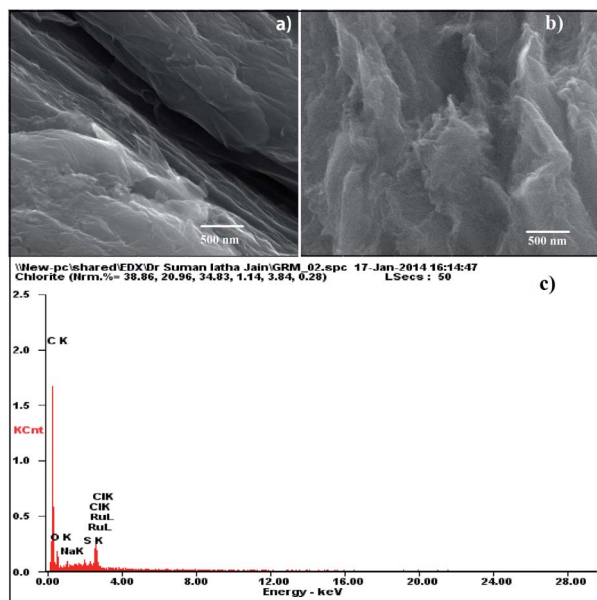Fig. 1   XRD patterns: (a) GO and (b) Ru–phen-GO **2**.

This journal is © The Royal Society of Chemistry 2014

J. Mater. Chem. A, 2014, **2**, 11246–11253 | **11247**

Fig. 2 SEM images of (a) GO and (b) Ru−phen-GO **2** and the (c) EDX pattern of **2**.
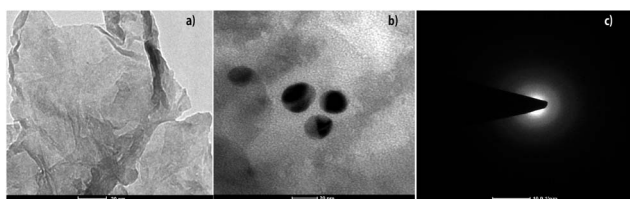

Fig. 3 TEM images of (a) GO and (b) Ru−phen-GO **2**, and the (c) SAED pattern of **2**.

and C–O–C bands, respectively.[16] Compared with the pure support GO, the strong band at 1680 cm^{-1}, assigned to amide groups (C=O–NH),[17] and a few peaks of ruthenium complex **1** at 1180 cm^{-1} and 1090 cm^{-1} clearly supported the successful attachment of complex **1** to GO.
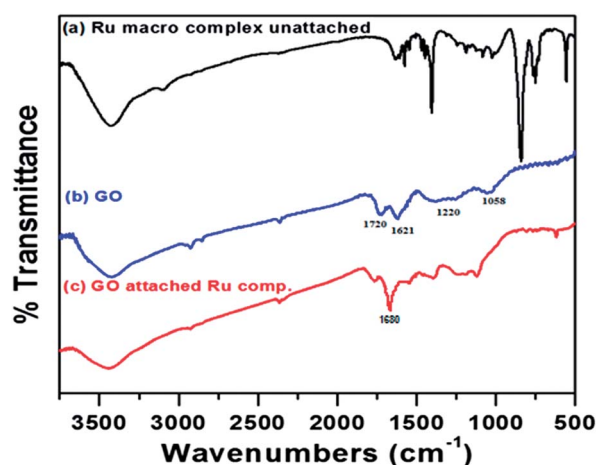
The UV-Vis absorption spectra of the ruthenium trinuclear complex **1**, GO and GO-immobilized complex **2** are shown in Fig. 5. The absorption spectrum of complex **1** (Fig. 5a) shows a sharp peak at 260 nm due to a $\pi \rightarrow \pi^*$ transition and a shoulder at 425 nm due to metal-to-ligand charge-transfer (MLCT).[18] The absorption spectrum of GO (Fig. 5b) indicates the characteristic absorption bands near to 230 nm due to the $\pi \rightarrow \pi^*$ transitions of aromatic ring electrons and a small hump near to 300 nm due to the $n \rightarrow \pi^*$ transitions of carbonyl group electrons.[19] After the immobilization of complex **1**, the absorption peak of GO exhibited a red shift at 300 nm (Fig. 5c). This was due to the coordination of the phenanthroline ligand to ruthenium complex **1**. Because of the large extent of the conjugated system in phenanthroline, the MLCT transition appeared at a low energy in the GO-supported complex.[20] Moreover, a red shift in the absorption spectrum of the GO-immobilized ruthenium complex confirmed the successful attachment of the ruthenium complexes to the GO support.

X-ray photoelectron spectroscopy (XPS) was used to further confirm the attachment of the Ru-complex to the phen-GO support. Fig. 6a depicts the survey spectrum of **2**, where the key elements such as Ru, N, O and C can be clearly identified. Furthermore, high-resolution XPS spectra at the C (1s) and Ru (3d) regions (Fig. 6b) revealed three prominent peaks at 284.76 eV, 281.94 eV and 285.85 eV, which are assigned to C (1s), Ru (3d$_{5/2}$) and Ru (3d$_{3/2}$) respectively, evidencing the successful immobilization of the ruthenium complexes on the GO support.[21]

The thermal stability of the developed photocatalyst **2** was determined by TGA (Fig. 7). The thermogram of GO (Fig. 7a) shows approx. 50% weight loss up to 400 °C. The first weight loss at 100 °C was due to the loss of water, and another major weight loss from 150 °C to 250 °C was due to the loss of oxygen-containing functionalities of GO.[22] The thermogram of **2** (Fig. 7b) shows a three-step weight loss pattern at temperatures ranging from 50 °C to 800 °C. The first weight loss at temperatures ranging from 50 °C to 250 °C was attributed to the removal of physically adsorbed water. The second region between 250 and 450 °C was due to the combustion of amine and unreacted oxygen-carrying functionalities, *i.e.* those not

Fig. 4 FTIR spectra of (a) Ru-complex **1**, (b) GO and (c) Ru−phen-GO **2**.
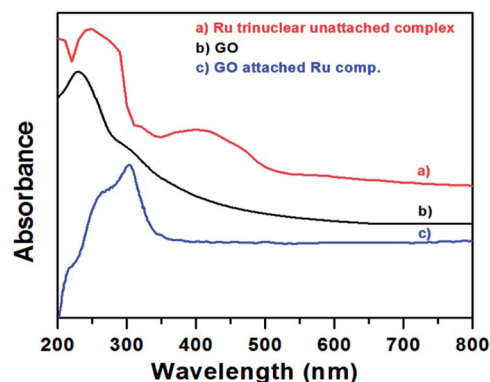

Fig. 5 UV-Vis absorption spectra of (a) Ru-complex **1**, (b) GO and (c) GO-attached complex **2**.
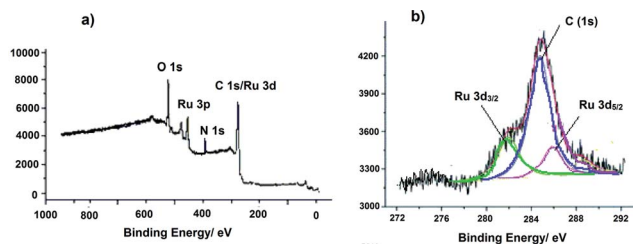
Fig. 6   XPS spectra: (a) a survey scan of Ru–phen-GO **2** and (b) C (1s) and Ru (3d).

used for attachment of the ruthenium complex. The third region was mainly related to the decomposition of the ligands of the ruthenium complexes in the temperature range from 450 to 800 °C.

The immobilization of ruthenium complex **1** on graphene oxide enhanced its photocatalytic activity significantly and provided absorption in the visible light region. This was further confirmed by determining the optical band gap of the synthesized graphene oxide with the help of a Tauc plot with linear extrapolation (Fig. 8). Owing to the amorphous nature and non-uniform oxidation levels of GO sheets, a sharp adsorption edge was not obtained in the Tauc plot. We observed an approximate band gap range between 2.9–3.7 eV, which is in good agreement with the existing literature reports.[9] The obtained band gap value of GO is quite large, and therefore the transition of the electrons from the valence band to the conduction band in visible light cannot be possible. However, the immobilization of the ruthenium complex moieties on the GO support provided an efficient visible light photocatalyst for CO_2 activation.[23]

The photocatalytic reduction of CO_2

First, the catalytic activity of GO and Ru–phen-GO was tested for the photoreduction of CO_2 in a water–DMF mixture, using triethylamine as a sacrificial donor under visible light irradiation. After the photoreduction, a 1 µl liquid sample was withdrawn and analyzed in a GC-FID equipped with a 30 m long Stabilwax® w/Integra-Guard® column. The methanol yield was used to evaluate the performance of the catalysts, as it was obtained as
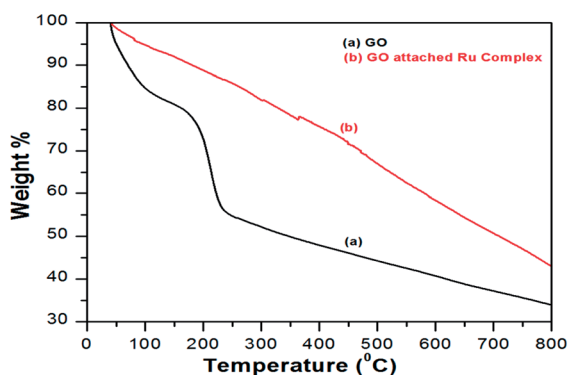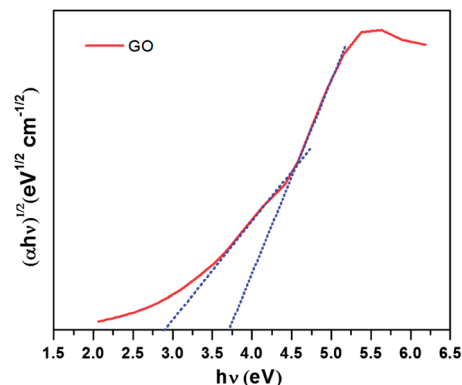

Fig. 8   Tauc plot for calculating the band gap of GO.

the major reduction product. The analysis of the gaseous phase did not show the presence of CO, CH_4 or any other possible product from the reduction of CO_2. Samples taken at different time intervals were analyzed by injecting them into the gas chromatograph with the help of an auto-sampler, followed by the quantitative measurement of their methanol yield. The methanol (MeOH) formation rate, R_{MeOH} (µmol g_{cat}^{-1}), was calculated as a function of the reaction time and plotted in Fig. 9. The results clearly indicated that the GO-immobilized Ru-complex exhibited a higher catalytic activity, compared to GO. After illumination for 48 h in visible light, using GO and GO-immobilized Ru-complex in the presence of triethylamine as sacrificial donor, the yields of methanol were found to be 2201.40 ± 8.76 and 3977.57 ± 5.60 µmol g_{cat}^{-1}, respectively. The higher yield of methanol using the GO-immobilized Ru-complex is attributed to the better dispersion of the ruthenium complexes attached to the sheets and the visible light-mediated electron transition in the complex, with the fast transfer of electrons to the conduction band of graphene oxide.

Blank experiments, in the absence of a photocatalyst under visible light irradiation, as well as in the dark using the GO-immobilized ruthenium complex under identical experimental conditions, showed that there was no organic product found for longer periods of exposure.

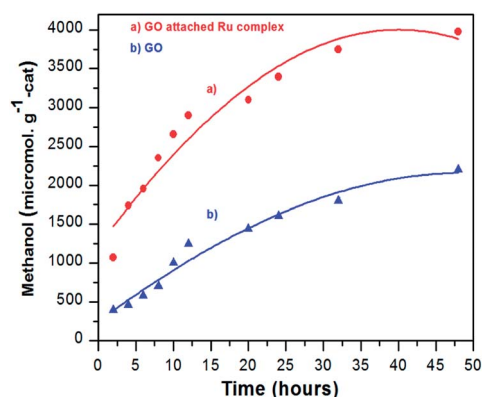Fig. 7   TGA plots of (a) GO and (b) Ru–phen-GO **2**.

Fig. 9   Conversion of CO_2 to methanol over time using (a) photocatalyst **2** and (b) GO.

This journal is © The Royal Society of Chemistry 2014

J. Mater. Chem. A, 2014, 2, 11246–11253 | 11249

Isotopic labeling experiments with $^{13}CO_2$

In order to confirm the methanol formation through CO_2 reduction, instead of the photo-dissociation of the solvent or graphene oxide support, isotopic labeling experiments were performed with $^{13}CO_2$. The photocatalytic experiment was carried out by using $^{13}CO_2$ in place of $^{12}CO_2$ under identical experimental conditions. The reaction product was analyzed by GC-MS. We obtained the distinct peak associated with $^{13}CH_3OH$ (m/z 33) instead of $^{12}CH_3OH$ (m/z 32) (Fig. S9†). These data confirmed that methanol was produced directly from the photocatalytic reduction of CO_2 instead of any photo-dissociation of the carbon-containing catalyst or solvent. Furthermore, a blank experiment without CO_2 under otherwise identical experimental conditions did not produce methanol.
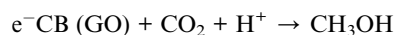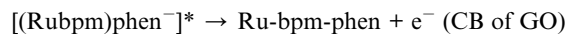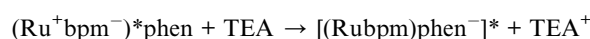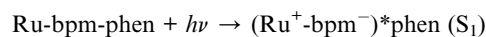
After the photocatalytic reaction, the catalyst was recovered by centrifugation and recycled for four subsequent runs under the described experimental conditions (Fig. 10). As shown in Fig. 10, the methanol yield was similar in all of the cases. These results confirmed the stability as well as the efficient recycling of the synthesized ruthenium complex immobilized to graphene oxide for the photoreduction of CO_2. Furthermore, ICP-AES analysis of the recovered catalyst showed that there was no significant leaching during the reaction, and the concentration of the ruthenium in the recovered catalyst was found to be 4.12 wt%. This is in good agreement with the concentration in the fresh catalyst (4.14%).

Moreover, the possible photocatalytic mechanism of the Ru–phen-GO has been demonstrated, for the better understanding of the CO_2 photoreduction process (Scheme 3). As shown in the Tauc plot, the wide band gap of GO restricts its excitation in visible light. However, the synthesized ruthenium complex can absorb strongly in the visible light region and be excited from the S_0 to S_1 state. In the synthesized complex, metal units are attached by bridging bipyrimidine (bpm) ligands, therefore the electron density of the conjugated π^* orbitals of the ligands decreases and electrons flow through the bridging ligands to another metal centre (the antenna effect).[24] Finally phen ligands
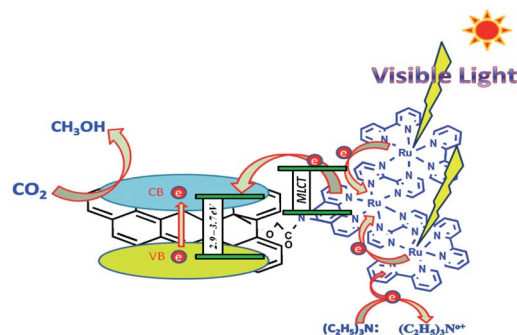
Scheme 3 Possible mechanism of the reaction.

inject electrons into the conduction band (CB) of GO, which are subsequently used for the reduction of adsorbed CO_2 to methanol on the surface of GO. Triethylamine acts as a sacrificial agent and provides electrons to the oxidized ruthenium for the continuation of the process.

$$Ru\text{-}bpm\text{-}phen + h\nu \rightarrow (Ru^+\text{-}bpm^-)^*phen\ (S_1)$$

$$(Ru^+bpm^-)^*phen + TEA \rightarrow [(Rubpm)phen^-]^* + TEA^+$$

$$[(Rubpm)phen^-]^* \rightarrow Ru\text{-}bpm\text{-}phen + e^-\ (CB\ of\ GO)$$

$$e^-CB\ (GO) + CO_2 + H^+ \rightarrow CH_3OH$$

Conclusions

We have synthesized a novel heterogeneous graphene-immobilized ruthenium trinuclear catalyst for the photocatalytic reduction of carbon dioxide to methanol under visible light irradiation. Owing to its wide band gap, graphene oxide alone does not undergo excitation in visible light. The ruthenium complex, because of its better visible light absorbance, facilitates the transportation of electrons from the ruthenium macromolecule to GO's conduction band. After 48 h of irradiation, the yield of methanol using the ruthenium complex immobilized to graphene oxide was found to be $3977.57 \pm 5.60\ \mu mol\ g_{cat}^{-1}$. This value is much higher than that of GO alone ($2201.40 \pm 8.76\ \mu mol\ g_{cat}^{-1}$). To the best of our knowledge, this is the first report describing the use of a graphene oxide-immobilized metal complex as an efficient photoredox catalyst for the photoreduction of CO_2. We believe that the results reported in the present work will open up new possibilities for developing efficient photocatalysts for the production of high value products from CO_2 in a sustainable way.
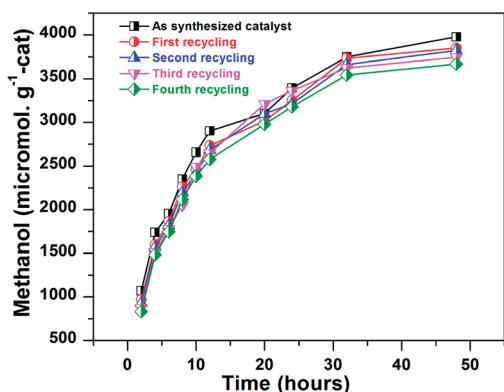
Fig. 10 Recycling of the Ru–phen-GO catalyst for the photoreduction of CO_2 to methanol.

Experimental

Materials

The 2,2′-bipyridine (bpy, 99%), graphite flakes, 2,2′-bipyrimidine (bpm, 95%), ruthenium chloride trihydrate and 1,10-phenanthroline-5-amine (phen-NH$_2$, 97%) purchased from Aldrich were of analytical grade and used without further purification. Ammonium hexafluoro phosphate (99.9%) and chloroacetic acid (99%) were of analytical grade and procured from Alfa Aesar. All other chemicals were of A. R. grade and used without further purification.

Techniques used

Fourier transform infrared spectra were recorded on a Perkin-Elmer spectrum RX-1 IR spectrophotometer using a potassium bromide window. Scanning electron microscopy (SEM) imaging of the synthesized GO for determining its rough structure was executed using a field emission scanning electron microscope (Jeol Model JSM-6340F). The fine structures of the materials were determined with high resolution transmission electron microscopy (HR-TEM), using an FEI-Tecnai G2 Twin transition electron microscope operating at an acceleration voltage of 200 kV. For HR-TEM, a very dilute aqueous dispersion of the catalyst was deposited on a carbon-coated copper grid. The absorption spectra of the unattached Ru-complex 1 in acetonitrile and the solid GO-attached Ru catalyst were collected on a Perkin Elmer lambda-19 UV-Vis-NIR spectrophotometer using a 10 mm quartz cell, and BaSO$_4$ as a reference. X-ray powder diffraction patterns were recorded on a Bruker D8 Advance diffractometer at 40 kV and 40 mA with Cu Kα radiation (λ = 0.15418 nm) for confirming the synthesis of GO and its functionalization, and the sample for XRD was prepared on a glass slide by adding the well-dispersed catalyst in a slot and drying properly. Surface properties like the Brunauer–Emmett–Teller (BET) surface areas, Barrett–Joiner–Halenda (BJH) porosities and pore volumes of GO and the GO-attached Ru-complex were examined by N$_2$ adsorption–desorption measurements at 77 K by using the VP; Micromeritics ASAP 2010. Thermogravimetric analyses (TGAs) of GO and the GO-attached Ru-complex, for evaluating the thermal stability of the catalyst, were carried out using a thermal analyzer TA-SDT Q-600. Analysis was carried out in the temperature range of 40 to 800 °C under nitrogen flow with a heating rate 10 °C min^{-1}. ^{1}H NMR and ^{13}C NMR spectra of the ruthenium complex were obtained at 500 MHz using a Bruker Avance-II 500 MHz instrument. To determine the ruthenium content of the catalyst, inductively coupled plasma atomic emission spectrometry (ICP-AES) analysis was carried out using an ICP-AE spectrometer (DRE, PS-3000UV, Leeman Labs Inc, USA). The metal from 0.05 g catalyst was leached out using conc. HNO$_3$, and the final volume was made up to 10 ml by adding distilled water. ESI-MS spectra of the synthesized ruthenium trinuclear complex 1 were recorded on a Thermo Exactive Orbitrap system in HESI mode. CHN analysis was done to confirm that metal had not leached and that the complex was intact during its synthesis.

Synthesis of graphene oxide

Graphene oxide (GO) was synthesized from graphite flakes using a modified Hummers method.[12] In a typical experiment, concentrated H$_2$SO$_4$ (68 ml) was added to a flask containing graphite flakes (2 g) and sodium nitrate (0.75 g) while stirring at 0 °C (ice bath). After that, KMnO$_4$ (9.0 g) was added slowly to this mixture and stirred for 5 days. 100 ml diluted H$_2$SO$_4$ (5 wt%) was added to this and heated at 90 °C for 2 hours with continuous stirring. The subsequent addition of 30 wt% H$_2$O$_2$ solution (approximately 5.4 ml) followed by stirring for 2 h at room temperature afforded graphene oxide, which was collected by centrifugation. The as synthesized material was subsequently washed with H$_2$SO$_4$ (3 wt%), H$_2$O$_2$ (0.5 wt%), HCl (3 wt%) and finally with distilled water.

Synthesis of carboxylated graphene oxide[25]

Graphene oxide (0.4 g) was dispersed in distilled water (200 ml) with the help of ultrasonication. The obtained suspension was treated with NaOH (2.4 g) and chloroacetic acid (2.0 g) and then sonicated for 3 h. This step converted the hydroxyl (–OH) and epoxy groups of GO to carboxylic acid groups (–COOH). Diluted HCl was added to the suspension containing GO–COOH to achieve a neutral pH. Finally the obtained GO–COOH was collected by centrifugation and washed with distilled water, and then dried.

Synthesis of phenanthroline (phen) ligand functionalized graphene oxide[10a,23]

Carboxylated graphene oxide (GO–COOH) was treated with thionyl chloride (25 ml) under reflux for 12 h to convert the carboxylic acid groups of GO into carbonyl chloride groups. After the completion of the reaction, excess thionyl chloride was removed under distillation at reduced pressure. The synthesized GO–COCl was washed with THF (3 times) and dried in a vacuum. The obtained GO–COCl was taken in DMF, treated with 1,10-phenanthroline-5-amine (phen-NH$_2$, 0.5 g) and triethyl amine (0.5 ml) and then refluxed under a nitrogen atmosphere for 18 h. Finally, the phenanthroline functionalized graphene oxide support (Phen-GO) was separated by centrifugation and washed thoroughly with ethanol, and dried under vacuum.

Synthesis of [Ru(bpy)$_2$bpm]·2PF$_6$ complex[26]

Ru(bpy)$_2$Cl$_2$·2H$_2$O[27] (1.0 g 2.0 mmol) and 2-2′-bipyrimidine (0.98 g, 6.2 mmol) were taken in a 100 ml round-bottomed flask and then a deoxygenated ethanol–water mixture was added (50 ml, 2 : 1 v/v), followed by refluxing for 3 h with stirring under a nitrogen atmosphere. After being cooled at room temperature, the mixture was treated with a saturated solution of ammonium hexafluorophosphate and then placed in a refrigerator at 0 °C to precipitate the complex. The precipitated complex was separated *via* membrane filtration and then dissolved in acetone, and re-precipitated with diethyl ether. The complex was further purified by column chromatography (alumina) using toluene–acetonitrile (3/2 v/v) as eluent (UV-Vis absorbance – 430, 286, 249 nm).

Synthesis of ruthenium trinuclear complex [{(bpy)$_2$Ru(bpm)]$_2$RuCl$_2$·4PF$_6$}] 1 [28]

In a typical experiment, [Ru(bpy)$_2$(bpm)](PF$_6$)$_2$ (0.865 mmol), RuCl$_3$·3H$_2$O (0.4605 mmol) and LiCl (4.715 mmol) were taken in a 100 ml round-bottomed flask and then ethanol was added (100 ml). The resulting mixture was refluxed with stirring for 24 h under a nitrogen atmosphere. The reaction mixture was cooled to room temperature and then a saturated solution of NH$_4$PF$_6$ was added to precipitate complex 1. For purification, the obtained complex was dissolved in the minimum amount of acetone and re-precipitated with diethyl ether. Further purification was done by column chromatography using alumina as the stationary phase and toluene–acetonitrile (v/v, 2 : 1) as a mobile phase. UV-Vis absorbance was found at λ max 425 nm and 260 nm. ESI-MS: 1827 [M$^+$ − 2Cl$^−$ + 2H$^+$], 1745 [M$^+$ − PF$_6$ − 6H$^+$], 1583 [M$^+$ − 2PF$_6$ − F$^−$], 1423 [M$^+$ − 3PF$_6$ − Cl$^−$ − 3H$^+$] and 1314[M$^+$ − 4PF$_6$ − 2H$^+$]. ^{1}H and ^{13}C NMR and ESI-MS spectra of the synthesized complex are shown in the ESI (Fig. S3–S6†).

Immobilization of complex 1 to the phen-GO support [29]

Phen-GO and the [(bpy)$_2$Ru(bpm)RuCl$_2$(bpm)Ru(bpy)$_2$](PF$_6$)$_4$ complex were added to a round-bottomed flask containing ethanol. The resulting suspension was refluxed in the dark under a N$_2$ atmosphere for 24 h. After being cooled at room temperature, the graphene oxide-immobilized ruthenium complex (Ru–phen-GO) 2 was separated by centrifugation and washed with ethanol until it became colorless, after the removal of the unreacted complex. ICP-AES analysis of the sample showed 4.1 wt% ruthenium in the synthesized heterogeneous material. Elemental analysis of the synthesized material showed C (%), 56.13; H (%) 3.20 and N (%) 4.43.

Photocatalytic CO$_2$ reduction experiment

The photocatalytic reduction was carried out under visible light by using a 20 watt white cold LED flood light (model no. -HP-FL-20W-F-Hope LED Opto-Electric Co. Ltd). The reaction vessel (dia. 5 cm) was kept about 3 cm away from the light source and the intensity of the light at the vessel was 85 W m^{-2}, as measured by an intensity meter. The vessel was initially charged with DMF (30 ml), triethylamine (10 ml) and deionized water (10 ml) and then the solution was degassed by purging with nitrogen for 30 min under vigorous stirring. Then the photocatalyst (0.1 g) was added and the resulting suspension was saturated with CO$_2$. The vessel was sealed, illuminated with a light source and the samples were collected at 2 h intervals. The samples were collected using a long needle and the catalyst was removed with the help of a syringe filter (2 nm PTFE, 13 mm diameter). The quantitative determination of methanol over time was performed using a gas chromatography-flame ionization detector (GC-FID) equipped with a 30 m long Stabilwax® w/ Integra-Guard® column, at a flow rate of 0.5 ml min^{-1}, an injector temperature of 250 °C and an FID temperature of 275 °C. A calibration curve was used for quantification and for the confirmation of the linear response of the GC-FID system (Fig. S7†). To evaluate the concentration of methanol produced as a result of the title reaction, 1.0 μl of the final reaction solution was used for the GC measurements. The concentration of methanol was calculated by integrating the peak area for the characteristic methanol band in the chromatogram (Fig. S8†).

Blank control experiments were conducted to ensure that methanol production was due to the photoreduction of CO$_2$, and to eliminate the surrounding interference. One blank test was carried out by illuminating the solution in the absence of the photocatalyst, and another was performed in the dark using a photocatalyst under identical experimental conditions. An additional blank test was performed by illuminating the reaction mixture in the presence of the photocatalyst by using N$_2$ rather than CO$_2$. No product was detected in the above three blank tests even after longer periods of exposure.

Notes and references

1 (a) A. J. Morris, G. J. Meyer and E. Fujita, *Acc. Chem. Res.*, 2009, **42**, 1983; (b) R. Reithmeier, C. Bruckmeier and B. Rieger, *Catalysts*, 2012, **2**, 544–571; (c) S. Naval, A. Dhakshinamoorthy, M. lvaro and H. Garcia, *ChemSusChem*, 2013, **6**, 562–577.

2 (a) S. N. Habisreutinger, L. Schmidt-Mende and J. K. Stolarczyk, *Angew. Chem., Int. Ed.*, 2013, **52**, 7372–7408; (b) Y. Ku, W.-H. Lee and W.-Y. Wang, *J. Mol. Catal. A: Chem.*, 2004, **212**, 191–196; (c) Y. Izumi, *Coord. Chem. Rev.*, 2013, **257**, 171–186; (d) F. Liao, Z. Zeng, C. Eley, Q. Lu, X. Hong and S. C. E. Tsang, *Angew. Chem.*, 2012, **124**, 5934–5938.

3 (a) H.-Y. Li, J. Wu, X.-H. Zhou, L.-C. Kang, D.-P. Li, Y. Sui, Y.-H. Zhou, Y.-X. Zheng, J.-L. Zuo and X.-Z. You, *Dalton Trans.*, 2009, 10563–10569; (b) J. Costamagna, G. Ferraudi, J. Canales and J. Vargas, *Coord. Chem. Rev.*, 1996, **148**, 221–248.

4 (a) X.-T. Zhou, H.-B. Ji and X.-J. Huang, *Molecules*, 2012, **17**, 1149–1158; (b) Z. Zhao, J. Fan, M. Xie and Z. Wang, *J. Cleaner Prod.*, 2009, **17**, 1025–1029; (c) Z. Wang, W. Mao, H. Chen, F. Zhang, X. Fan and G. Qian, *Catal. Commun.*, 2006, **7**, 518–522.

5 A. K. Geim and K. S. Novoselov, *Nat. Mater.*, 2007, **6**, 183–191.

6 (a) X.-F. Zhang and Q. Xi, *Carbon*, 2011, **49**, 3842–3850; (b) X. Zhang, L. Hou, A. Cnossen, A. C. Coleman, O. Ivashenko, P. Rudolf, B. J. vanWees, W. R. Browne and B. L. Feringa, *Chem.–Eur. J.*, 2011, **17**, 8957–8964; (c) A. Adan-Mas and D. Wei, *Nanomaterials*, 2013, **3**, 325–356.

7 (a) K. P. Loh, Q. Bao, P. K. Ang and J. Yang, *J. Mater. Chem.*, 2010, **20**, 2277–2289; (b) V. Singh, D. Joung, L. Zhai, S. Das, S. I. Khondaker and S. Seal, *Prog. Mater. Sci.*, 2011, **56**, 1178–1271; (c) H. Bai, C. Li and G. Shi, *Adv. Mater.*, 2011, **23**, 1089–1115.

8 L. Dai, D. W. Chang, J.-B. Baek and W. Lu, *Small*, 2012, **8**, 1130–1166.

9 H.-C. Hsu, I. Shown, H.-Y. Wei, Y.-C. Chang, H.-Y. Du, Y.-G. Lin, C.-A. Tseng, C.-H. Wang, L.-C. Chen, Y.-C. Lind and K.-H. Chen, *Nanoscale*, 2013, **5**, 262–268.

10 (a) R. Yamuna, S. Ramakrishnan, K. Dhara, R. Devi, N. K. Kothurkar, E. Kirubha and P. K. Palanisamy, *J.*

Nanopart. Res., 2013, **15**, 1399; (*b*) X. Zhang, Y. Feng, S. Tang and W. Feng, *Carbon*, 2010, **48**, 211–216; (*c*) S. Li, X. Zhong, H. Yang, Y. Hu, F. Zhang, Z. Niu, W. Hu, Z. Dong, J. Jin, R. Li and J. Ma, *Carbon*, 2011, **49**, 4239–4245.

11 (*a*) W.-W. Yang, Y.-W. Zhong, S. Yoshikawa, J.-Y. Shao, S. Masaoka, K. Sakai, J. Yao and M. Haga, *Inorg. Chem.*, 2012, **51**, 890–899.

12 W. S. Hummers and R. E. Offeman, *J. Am. Chem. Soc.*, 1958, **80**, 1339.

13 IUPAC Recommendations, *Pure Appl. Chem.*, 1994, **66**, 1739.

14 S. Bose, T. Kuila, A. K. Mishra, N. H. Kim and J. H. Lee, *J. Mater. Chem.*, 2012, **22**, 9696–9703.

15 Y. Zhang, X. Sun, L. Pan, H. Li, Z. Sun, C. Sun and B. K. Tay, *J. Alloys Compd.*, 2009, **480**, L17–L19.

16 (*a*) Y. Xu, H. Bai, G. Lu, C. Li and G. Shi, *J. Am. Chem. Soc.*, 2008, **130**, 5856; (*b*) L. Xiaolin, Z. Guangyu, B. Xuedong, S. Xiaoming, W. Xinran, W. Enge and D. Hongjie, *Nat. Nanotechnol.*, 2008, **3**, 538.

17 X. Zhang, Y. Feng, P. Lv, Y. Shen and W. Feng, *Langmuir*, 2010, **26**, 18508–18511.

18 Y. Fuchs, S. Lofters, T. Dieter, W. Shi, R. Morgan, T. C. Strekas, H. D. Gafney and A. D. Baker, *J. Am. Chem. Soc.*, 1987, **109**, 2691.

19 V. H. Pham, T. V. Cuong, S. H. Hur, E. W. Shin, J. S. Kim, J. S. Chung and E. J. Kim, *Carbon*, 2010, **48**, 1945.

20 R. M. Berger, *Inorg. Chem.*, 1990, **29**, 1920.

21 X. You, G. Zou, Q. Ye, Q. Zhang and P. He, *J. Mater. Chem.*, 2008, **18**, 4704–4711.

22 C. Mattevi, G. Eda, S. Agnoli, S. Miller, K. A. Mkhoyan, O. Celik, D. Mastrogiovanni, G. Granozzi, E. Garfunkel and M. Chhowalla, *Adv. Funct. Mater.*, 2009, **19**, 2577–2583.

23 Y. Yu, M. Zhou, W. Shen, H. Zhang, Q. Cao and H. Cui, *Carbon*, 2012, **50**, 2539–2545.

24 (*a*) G. Eda, C. Mattevi, H. Yamaguchi, H.-K. Kim and M. Chhowalla, *J. Phys. Chem. C*, 2009, **113**, 15768–15771; (*b*) C. Kleverlaan, M. Alebbi, R. Argazzi, C. A. Bignozzi, G. N. Hasselmann and G. J. Meyer, *Inorg. Chem.*, 2000, **39**, 1342; (*c*) R. Argazzi, N. Y. M. Iha, H. Zabri, F. Odobel and C. A. Bignozzi, *Coord. Chem. Rev.*, 2004, **248**, 1299; (*d*) T. A. White, J. D. Knoll, S. M. Arachchige and K. J. Brewer, *Materials*, 2012, **5**, 27–46.

25 X. Sun, Z. Liu, K. Welsher, J. T. Robinson, A. Goodwin, S. Zaric and H. Dai, *Nano Res.*, 2008, **1**, 203–212.

26 G. N. A. Nallas, S. W. Jones and K. J. Brewer, *Inorg. Chem.*, 1996, **35**, 6974–6980.

27 B. P. Sullivan, D. J. Salmon and T. J. Meyer, *Inorg. Chem.*, 1978, **17**, 3334.

28 M. M. Richter and K. J. Brewer, *Inorg. Chem.*, 1993, **32**, 5762.

29 M. Kobayashi, S. Masaoka and K. Sakai, *Molecules*, 2010, **15**, 4908–4923.